A Stapled Peptide Inhibitor of METTL3-METTL14 for Cancer Therapy

Zenghui Li[1,2,#], Yuqing Feng[1,3,#], Hong Han[1,2], Xingyue Jiang[1,2], Weiyu Chen[1,2], Xuezhen Ma[1], Yang Mei[1], Xuhui Yan[4], Ping Yin[4], Dan Yuan[1,2], Dingxiao Zhang[1,3,*], Junfeng Shi[1,2,3,*]

[1] Hunan Provincial Key Laboratory of Animal Models and Molecular Medicine, State Key Laboratory of Chemo/Bio-Sensing and Chemometrics, School of Biomedical Sciences, Hunan University, Changsha, Hunan 410082, China

[2] Greater Bay Area Institute for Innovation, Hunan University, Guangzhou 511300, Guangdong Province, China

[3] Shenzhen Research Institute, Hunan University, Shenzhen 518000, Guangdong Province, China

[4] National Key Laboratory of Crop Genetic Improvement, Hubei Hongshan Laboratory, Huazhong Agricultural University, Wuhan, 430070, China.

[#]These authors contribute equally

Corresponding Authors: **zdx1980@hnu.edu.cn, Jeff-Shi@hnu.edu.cn**

Abstract

METTL3, a primary methyltransferase catalyzing RNA m^6A modification, has been identified as an oncogene in several cancer types and thus nominated as a potentially effective target for therapeutic inhibition, although current options using this strategy are limited. In this study, we targeted protein-protein interactions at the METTL3-METTL14 binding interface to inhibit complex formation and subsequent catalysis of RNA m^6A modification. Among candidate peptides, **RM3** exhibited the highest anti-cancer potency, inhibiting METTL3 activity while also facilitating its proteasomal degradation. We then designed a stapled peptide inhibitor (**RSM3**) with enhanced peptide stability and formation of the α-helical secondary structure required for METTL3 interaction. Functional and transcriptomic analysis *in vivo* indicated that **RSM3** induced upregulation of programmed cell death-related genes while inhibiting cancer-promoting signals. Furthermore, tumor growth was significantly suppressed while apoptosis was enhanced upon **RSM3** treatment, accompanied by increased METTL3 degradation and reduced global RNA methylation levels in two *in vivo* tumor models. This peptide inhibitor thus exploits a mechanism distinct from other competitive-binding small molecules to inhibit oncogenic METTL3 activity. Our findings collectively highlight the potential of targeting METTL3 in cancer therapies through peptide-based inhibition of complex formation and proteolytic degradation.

Introduction

N6-methyladenosine (m^6A) is a prevalent RNA modification that plays essential regulatory roles to coordinate a wide range of biological processes, including RNA splicing, stability, and translation[1, 2]. Dysregulation of m6A modification has been firmly linked to the development and progression of various diseases (*e.g.,* cancers)[3]. Installation of m^6A modifications requires the methyltransferase activity catalyzed by the METTL3-METTL14 complex, the former protein serving as the catalytic subunit, while the latter performs RNA-binding function; by contrast, m6A removal is mediated by m^6A demethylases, such as FTO and ALKBH5[4]. Complex formation is essential for m6A methyltransferase function, and m6A modification is largely lost in the absence of METTL3-METTL14 heterodimerization[5, 6]. Numerous studies have shown that METTL3 is expressed at aberrantly high levels in several cancer types, suggesting a prominent role in cancer progression[7, 8], and has been shown to positively regulate cancer development by promoting metastasis and tumor growth in malignancies such as acute leukemia[9], liver cancer[10], stomach cancer[11], lung cancer[12], colorectal cancer[13], and prostate cancer[14]. Conversely, other studies have shown that cancer cell growth is dramatically inhibited upon METTL3 knockdown, suggesting its potential as a therapeutic target for treating various cancers [15, 16, 17].

Although the crystal structure of the METTL3-METTL14 complex has been solved since 2016[18], progress in developing METTL3 inhibitors has been limited, with the METTL3 substrate co-factor, S-Adenyl-methionine (SAM), which is required for methyl group transfer, serving as the most common target for inhibitor design. For example, Kouzarides and co-workers identified the small molecule METTL3 inhibitor, **STM2457**, which displayed high potency against acute myeloid leukemia in high-throughput screens, but still lacks experimental validation of its efficacy against solid tumors [19]. Although other competitive and non-competitive inhibitors that are structurally similar to SAM, such as Sinefungin[20], UZH2[21], and Eltrombopag[22], have been shown to exhibit substantial suppression of cancer cell growth, the *in vivo* efficacy of these small molecules requires further investigation. Thus, METTL3 is well-established as a viable potential target for cancer therapies, but the lack of available options in clinic suggests an urgent need for further development of effective METTL3-targeting treatment strategies [23].

As an alternative to small molecules, peptides offer a versatile and potentially powerful approach for targeted inhibition of proteins, especially through competitive disruption of protein-protein interactions (PPIs) by mimicking peptide binding epitopes[24, 25, 26, 27]. Peptide drugs have been extensively developed for several diseases such as diabetes, and show high potential for clinical application[28, 29]. Here, in this work, we developed a series of peptide-based inhibitors targeting METTL3 through a rational design strategy with subsequent modification to enhance specific properties. Among the candidates, one peptide targeting a binding site on METTL3 required for complex assembly with METTL14 showed the highest potency against a panel of cancer cells, leading to our subsequent engineering of its affinity and stability, especially through Bis(bromomethyl)biphenyl (bph)-based stapling. This final peptide inhibitor, **RMS3,** exhibited high efficacy in inhibiting the growth of multiple cancer cell lines, including prostate cancer (*e.g.* PC3 and DU145),

leukemia (*e.g.* CEM), and lung cancer (*e.g.* A549). Furthermore, **RMS3** could both disrupt METTL3-METTL14 complex formation as well as induce its subsequent proteasomal degradation, globally inhibiting m6A modification in cancer cells. As the first-in-class peptide inhibitor targeting METTL3, **RMS3** utilizes a markedly distinct mechanism of action from that of small molecule inhibitors, supported by *in vitro* and *in vivo* validation of its cytotoxicity and anti-tumor effects in multiple cancer cell lines and xenograft tumor models. Our study thus provides a promising therapeutic approach to treat a variety of tumor types, particularly prostate cancer, as well as a design strategy for developing new peptide-based drugs for other METTL3-dependent diseases or other therapeutic targets.

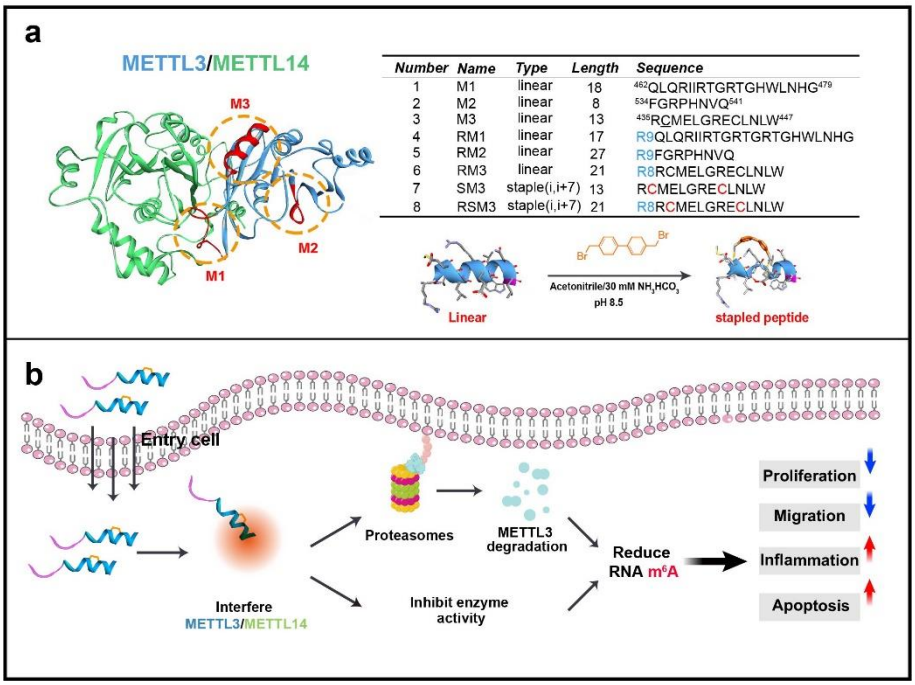

Figure 1. (a) Model of the METTL3-METTL14 complex crystal structure illustrating protein-protein interaction (PPIs; yellow dashed circles) at the binding interface and the peptide sequences designed to target and disrupt these PPIs in M1, M2, and M3 regions (right). (b) Further optimization through peptide stapling technology enabled construction of **RMS3**, increasing the potency of peptide inhibitory effects on cancer cell proliferation, migration, and tumor growth. The amino acids highlighted (**M3**, **RCMELGRECLNLW**) with underlining, which underwent mutation from **A** to **C** in the original sequence, were used to construct stapled peptides.

Results and discussion

Peptide inhibitor design and validation

Using previously reported crystal structure of the METTL3-METTL14 complex[18], we identified three distinct domains potentially essential for protein-protein interactions (PPIs) required for complex formation, suggesting their strong potential as targets for peptide-based inhibition of METTL3 activity. Following this rationale, the **RM1**, **RM2**, and **RM3** candidate peptides were respectively designed to target the M1 (RNA-binding groove), M2 (catalytic core), and M3 (METTL3/14 interface) regions of the complex, and fused each

peptide to the classic cell-penetrating peptide, R9 (RRRRRRRRR), to enhance cellular penetration (**Fig. 1 & Fig.S1**) [30, 31]. Among the functional regions targeted for interference, **RM1** was designed to interact with the methylase catalytic core which binds to the SAM catalytic substrate; **RM2** is predicted to disrupt interactions between METTL3-METTLE14 and mRNA, incorporating sequence from the RNA-binding grooves; and **RM3** was derived from an α-helix located at the METTL3-METTL14 interface and intended to destabilize complex formation and block protein function. The detailed molecular mechanism(s) and regulatory network (METTL3/m6A/RRBP1) of METTL3 in promoting cancer progress in prostate cancer is described in a parallel study [FYQ-paper]. Considering that METTL3 is highly upregulated in PCa cells and plays a significant role in cancer development, we assessed the potency of peptide inhibitors using MTT assays with PC3 and DU145 cell lines. As shown in **Fig. 2a and 2b, RM1** and **RM2** exhibited relatively modest cytotoxicity, while **RM3** displayed substantially greater anticancer effects, with IC_{50} values of 35.4 μM and 55.3 μM against PC3 and DU145 cells, respectively. Further evaluation through long-term clonogenic assays (**Fig. 2c and 2d**) confirmed that **RM3** exerted stronger inhibitory effects than either **RM1** or **RM2**. These findings supported the further exploration of **RM3** as a promising candidate anticancer drug warranting further optimization.

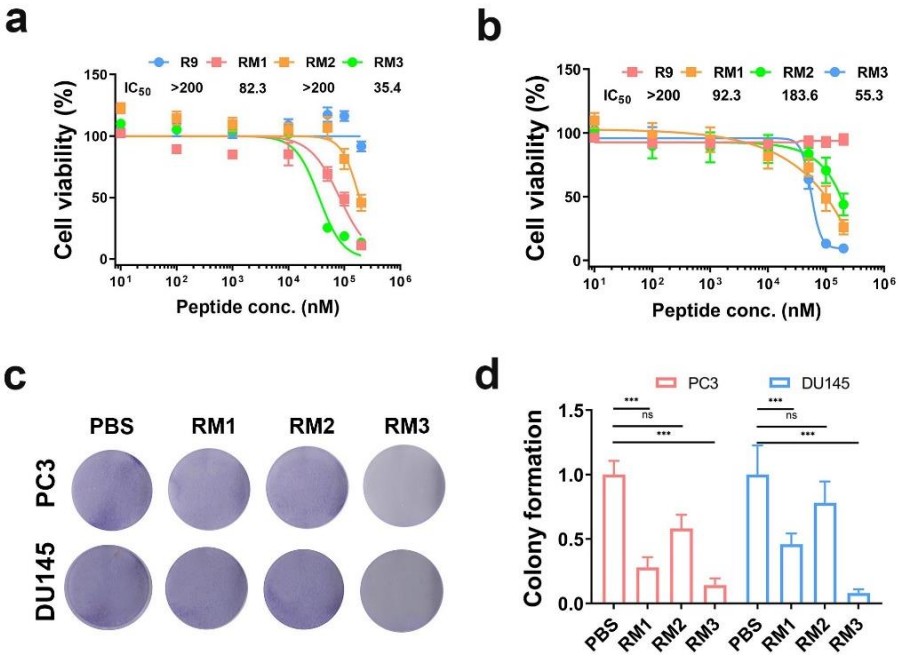

Figure 2. Evaluation of peptide inhibitors. Cytotoxicity of peptide inhibitors against the **(a)** PC3 and **(b)** Du145 cell lines. Clone formation plate assays **(c)** and quantification **(d)** to assess the peptide effects on growth and proliferation in prostate cancer cells (n=3). For a-d mean and error (±s.d.) were obtained from at least three replicates. One-way analysis of variance (ANOVA) with Tukey's test correction was used in statistical analysis test. *P < 0.05, **P < 0.01, ***P < 0.005, and not significant by P > 0.05.

Physicochemical properties and activity of M3 derivatives *in vitro*

To enhance the effects of the **M3** peptide, we employed peptide stapling, a well-established technique for increasing peptide stability and activity by covalently linking two specific amino acids (*e.g.* Cysteine)[32]. In this work, we utilized this strategy to generate the **SM3**

and **RSM3** stapled peptides from **M3** and **RM3**, respectively (See synthetic routes in **Fig S2.**). The binding affinity of stapled peptides was evaluated through microscale thermophoresis (MST) assays, which measure interaction strength between peptides and their target protein. Notably, **SM3** exhibited high affinity binding to the METTL3-METTL14 complex, with a K_d value of 4.25 μM. In comparison, the non-stapled peptide, **M3,** displayed markedly lower affinity (K_d = 90.1 μM). This significant improvement in binding affinity was likely due to the higher stability secondary structure of the stapled peptide (**Fig. 3a**). Circular dichroism (CD) measurements further verified that **SM3** could adopt an α-helix conformation in solution, whereas the non-stapled **M3** peptide fragment was mainly found in a random coil conformation (**Fig. 3b**).

Functional assays demonstrated that **SM3** could effectively inhibit METTL3-METTL14 complex transferase activity. More specifically, METTL3 methyltransferase activity was decreased by 63% in the presence of **SM3**, but decreased by 52% upon exposure to **M3**, further indicating the higher potency of the stapled peptide (**Fig. 3c**). Stability assays indicated that **RSM3** exhibited substantially higher biostability when treated with a 15% fetal bovine serum (FBS) solution, retaining ~41.8% of its initial concentration after 360 min of incubation, while the **RM3** linear peptide was completely degraded within 180 min (**Fig. 3d**). This stability could be attributed to the structural integrity conferred by the stapling strategy. In addition, we evaluated possible hemolytic activity by the peptide to assess its potential cytotoxicity towards human blood cells. In primary human blood cells, the peptide inhibitor showed no obvious toxicity at concentrations up to 200 μM after 24 h of incubation (**Fig. 3e)**. Collectively, these findings highlight the improved binding affinity, biostability, and activity that are inherently linked to a highly stable α-helical conformation resulting from peptide stapling. We therefore further explored the development of **RSM3** as a promising anti-cancer drug candidate.

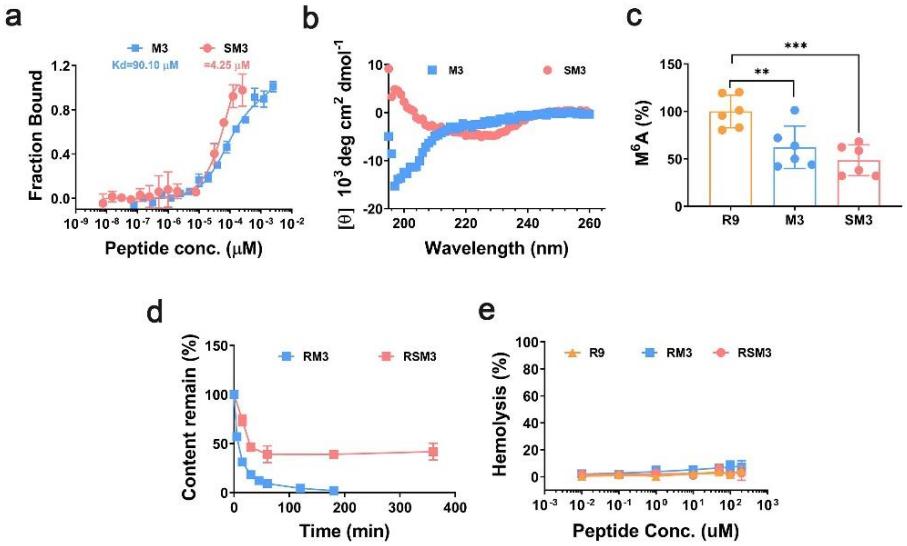

Figure 3. Physicochemical characterization of peptide inhibitors. **(a)** Microscale thermophoresis (MST) assays measuring the binding affinity between peptide inhibitors and METTL3–METTL14 complex, and **(b)** circular dichroism (CD) spectra scanning of **SM3** (red) and **M3** (blue) to determine peptide secondary structure. **(c)** Peptide effects on METTL3–METTL14 methyltransferase activity *in vitro* (n=5). **(d)** Serum

stability of **RSM3** and **RM3** over time in the presence of 15% FBS. **(E)** Hemolysis assays with primary human blood cells evaluating the hemolytic potential of **R9**, **RM3** and **RSM3**. For **a,c-e** mean and error (±s.d.) were obtained from at least three replicates. One-way analysis of variance (ANOVA) with Tukey's test correction was used in statistical analysis test. *P < 0.05, **P < 0.01, ***P < 0.005, and not significant by P > 0.05.

Evaluation of RSM3 anti-cancer effects

To evaluate the therapeutic or anti-cancer effects of the **RSM3** stapled peptide, its general cytotoxicity was assessed in a panel of ten cancer cell lines. The results showed that both **RSM3** and **RM3** exhibited broad toxicity towards various cancer cells including PC3, DU145, HeLa, HepG2, HCT116, A549, K562, MDS-L, CCRF-CEM (**Fig. S3**). It is noteworthy that the IC_{50} of **RSM3** towards the leukemia cell line, CCRF-CEM, was approximately 4.6 ± 1.03 μM. Following our initial experiments, further investigation of **RSM3** activity focused on the prostate cancer models. As expected, the **RSM3** stapled peptide displayed higher toxicity, with lower IC_{50} values, than the non-stapled **RM3** peptide (25.8 ± 1.9 μM *vs* 55.3 ± 2.4 μM, **RSM3** *vs* **RM3**) in the DU145 cell line (**Fig.4a**). Cell migration (Trans-well) and colony formation assays showed the potent inhibitory effects of **RSM3** and **RM3** on cancer cell aggressiveness compared to the control peptide R9. Treatment with either **RSM3** or **RM3** resulted in approximately 2~3 fold less cell migration and a ~20-fold reduction in PC3 or DU145 colony formation **(Fig. 4b&c)**.

We next investigated the cytotoxic effect of peptide inhibitors. To better understand the impacts on cell proliferation, we employed EdU labeling with confocal laser scanning microscopy (CLSM) to assess the proportion of cancer cells that entered the S phase of the cell cycle. Image analysis indicated that PCa cells in the **RSM3** and **RM3** treatment groups exhibited significantly weaker EdU signal, ~35.0% and ~47.0% that of the PBS control group (**Figure 4d&e)**, indicating that cell proliferation was markedly reduced in the presence of these peptides. Additionally, flow cytometry analysis revealed that ~29.2% of PC3 cells and 16.9% of DU145 treated with **RSM3** were arrested in the sub-G1 phase, compared to ~8.5% and ~3.6% for PC3 and DU145 cells, respectively, in the PBS group (**Fig. S4**). These findings suggested that **RSM3** could effectively induce cell cycle arrest. Subsequently, Annexin V-FITC and TUNEL staining was performed to evaluate apoptosis levels associated with **RSM3** or **RM3** treatment. TUNEL assays clearly showed that **RSM3** could induce higher levels of apoptosis than **RM3**, although apoptosis levels in the RM3 treatment group were also significantly higher than in controls (**Fig. 4f**). Quantification by flow cytometry indicated that 60% of PC3 cells and ~30% of DU145 entered apoptosis in the **RSM3** group, compared to 4% and ~5% of PBS-treated PC3 and DU145 cells, respectively (**Fig. 4g**). Furthermore, a larger proportion of apoptotic cells were in the late stage, accounting for ~90% of the total apoptotic PC3 cells. The proportion of cells with apoptosis induced by **RSM3** was approximately 2-fold higher than that of **RM3**, further supporting the higher toxicity of the stapled peptide towards cancer cells. Western blot assays confirmed that cleaved caspase-3 accumulated in peptide-treated cells (**Fig. S5**), further validating the apoptotic effect. Collectively, these results illustrated the anticancer activity of METTL3 peptide inhibitor by inducing cell apoptosis and cell cycle arrest.

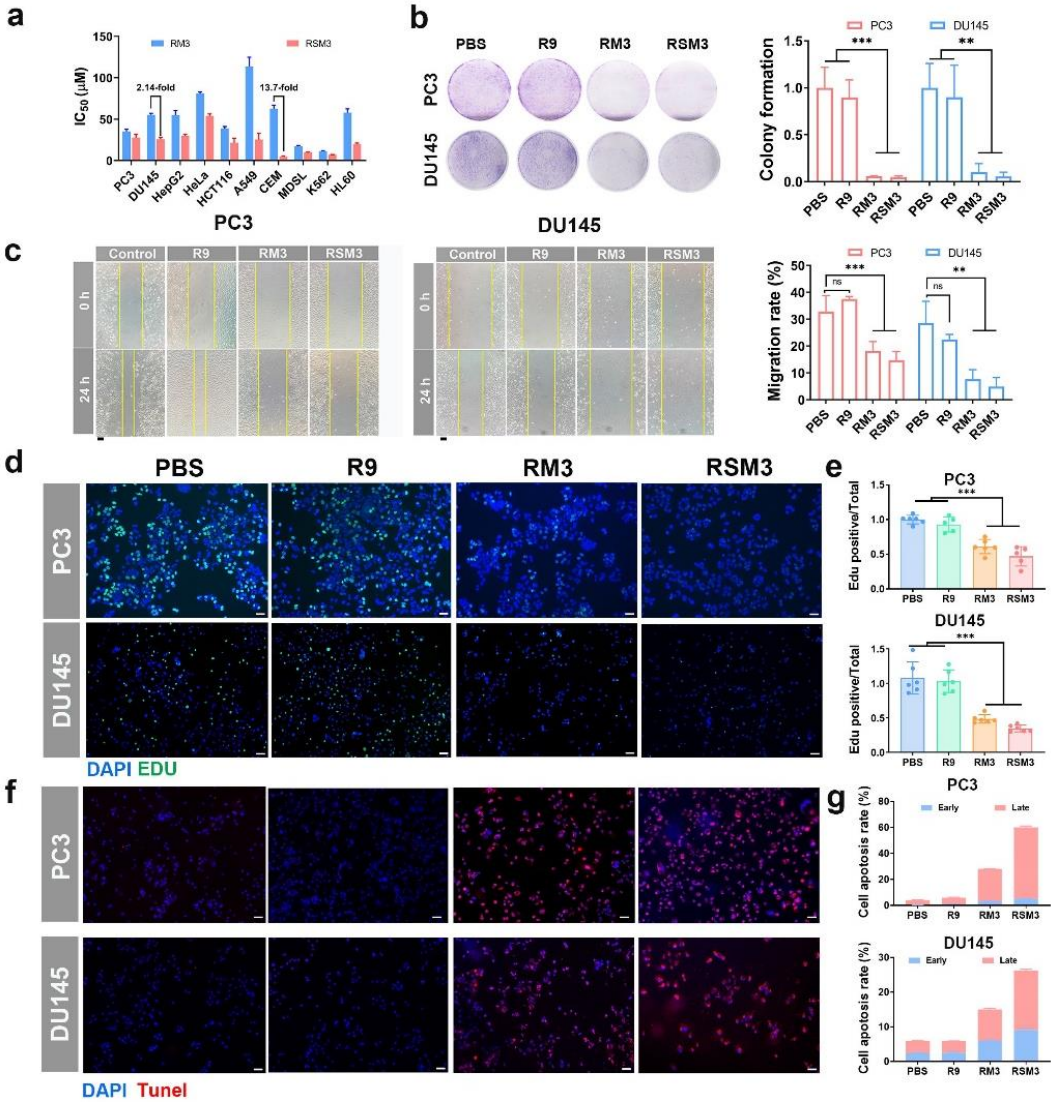

Figure 4. Evaluation of cytotoxic effects by METTL3-METTL14-targeting peptides. **(a)** MTT assays evaluating cell viability. (b) Colony formation assays and **(c)** cell migration assays in PCa cell lines (n=3). Scale bar: 20 μm. **(d)** Representative images of EdU labeling to assess cell proliferation. **(e)** Quantification of EdU staining. **(f)** TUNEL staining and **(g)** flow cytometry analysis of apoptosis levels in peptide-treated DU145 and PC3 cells. For **a-e** mean and error (±s.d.) were obtained from at least three replicates. One-way analysis of variance (ANOVA) with Tukey's test correction was used in statistical analysis test. *P < 0.05, **P < 0.01, ***P < 0.005, and not significant by P > 0.05.

RSM3 interaction with METTL3-METTL14 decrease complex stability and function

To explore the interactions between the peptide inhibitor and METTL3, we used a FITC-labeled fluorescent **RM3** to track its intracellular localization (**Fig. 5a**). CLSM image analysis illustrated the obvious and rapid cellular uptake of **RM3**, in contrast with the minimal cellular entry observed with the **M3** control peptide lacking R9 (**Fig. S6**). This result could at least partially explain the markedly lower inhibitory effects of **M3** and **SM3** towards cancer cells compared to that of **M3** or even **SM3** in combination with the R9 cell penetration peptide. Immunostaining for METTL3 confirmed that fluorescent signal from **RSM3** co-localized with that of METTL3 (**Fig. 5b**), while co-staining for METTL3 and METTL14 revealed that both proteins were obviously localized to the perinuclear region at 6 h of **RSM3** treatment **(Fig. 5c)**[33]. Furthermore, METTL3 and METTL14 signal intensity were both decreased, suggesting that treatment with **RSM3** could potentially result in altered function and possible degradation of the METTL3-METTL14 complex. Western blot analysis further confirmed that METTL3 and METTL14 levels were reduced in PC3 cells at 12 h of **RSM3** treatment (**Fig. 5d**), supporting that **RSM3** could both inhibit catalytic activity and also trigger degradation of the METTL3-METTL14 complex.

Subsequent RNA blot assays with m^6A ELISA demonstrated that m6A modifications were significantly reduced in PC3 or DU145 cells treated with **RSM3** or **RM3**, reaching levels approximately ~20% that detected in the R9 and PBS treatment groups (**Fig. 5e&f**). These results highlighted the potent effects of inhibiting METTL3 methyltransferase activity with stapled **M3** peptides. We next investigated the impact of peptide inhibitors on METTL3 half-life by pre-treating PC3 cells with cycloheximide (CHX) to block protein synthesis prior to **RSM3** or **RM3** administration. Western blots showed that **RSM3** or **RM3** treatment resulted in dramatically reduced half-life for METTL3 (**Fig. 5g**). Subsequent examination of the **RSM3**-associated degradation pathway through treatment with autophagy inhibitor (chloroquine, CQ) or proteasome inhibitor (MG132) revealed that exposure to MG132, but not CQ, could reverse the depletion of METTL3 in the **RSM3**-treated cells. By contrast, treatment with the METTL3 inhibitor, **STM2457**, had no influence on METTL3 levels in WB analysis. These results indicated that **RSM3** treatment could activate METTL3 degradation through the proteasome pathway, different from the inhibitory activity of **STM2457** on METTL3 methyltransferase activity. Taken together, these results indicated that interference in METTL3-METTL14 interaction by **RSM3** or **RM3** could block m6A modification while also inducing the proteasomal clearance of METTL3 in prostate cancer cells, and further suggested that the stapled **RSM3** peptide might be an effective candidate drug for cancer therapy.

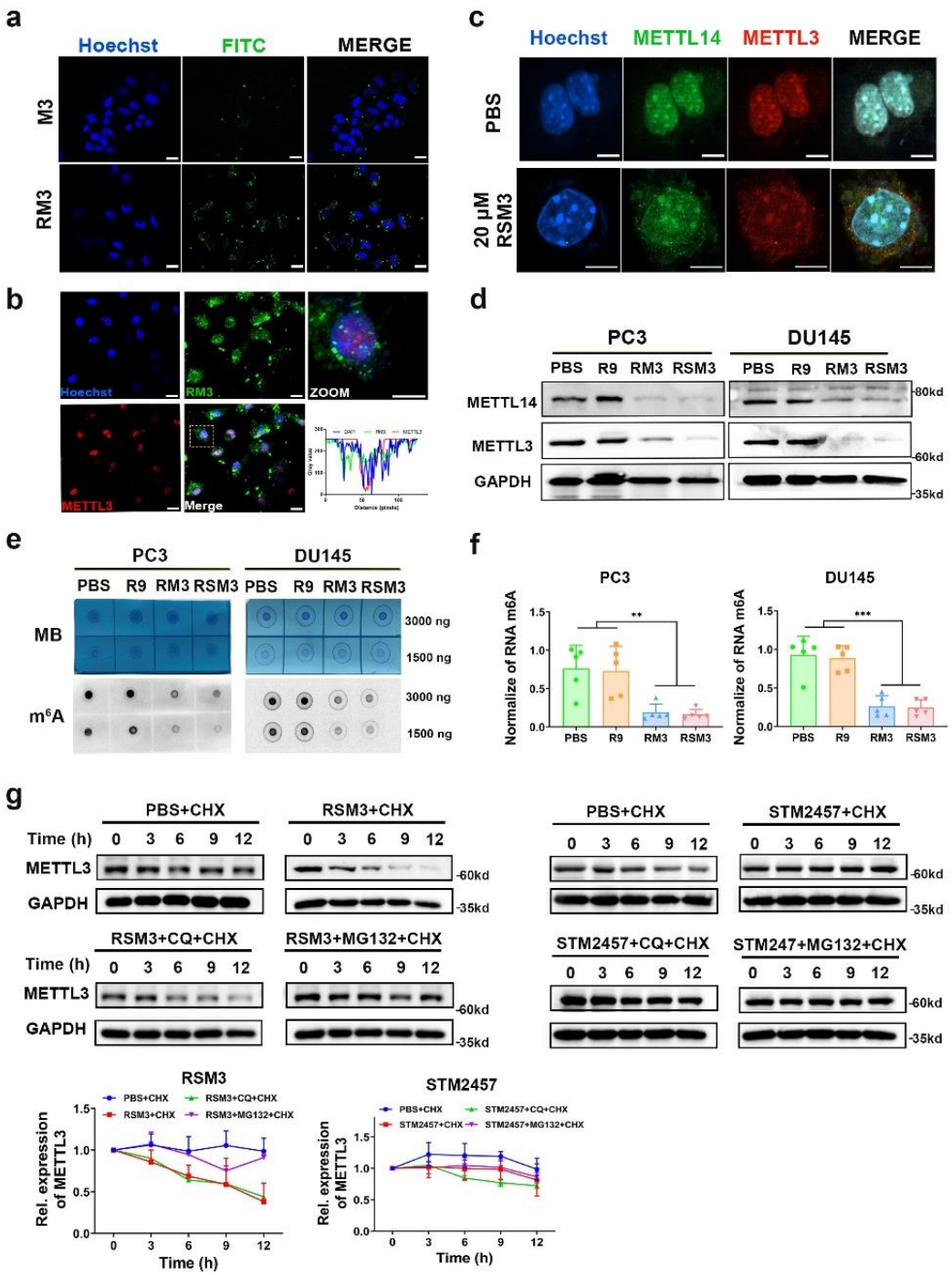

Figure 5. Peptide inhibitors modulate METTL3 stability and function. **(a)** Representative confocal microscopy images of PC3 cells treated with 10 μM FITC-labeled **M3** or **RM3** showing differences in cellular uptake in the presence or absence of R9 CPP. **(b)** Immunostaining for METTL3 to detect co-localization with FITC-labeled **RM3**. **(c)** Immunostaining for METTL3 and METTL14 in PC3 cells treated with **RSM3** and PBS vehicle control.**(d)** Western blot analysis to detect METTL3 or METTL14 in PC3 cells treated 25 μM **RSM3** over 12 h. **(e)** RNA blot analysis demonstrating the impact of peptide inhibitor on m^6A methylation level in PC3 and DU145 cells treated with 25 μM of **RSM3** over 12 h, Methylene blue (MB). **(f)** ELISA analysis of m^6A modification levels in PC3 and DU145 cells treated with **RM3, RSM3,** R9, or PBS controls. **(g)** Western blotting analysis demonstrating the degradation of METTL3 mediated through proteasome pathway upon the treatment with CHX or STM132 and 25 μM **RSM3** over 12 h. For

f,g mean and error (±s.d.) were obtained from at least three replicates. One-way analysis of variance (ANOVA) with Tukey's test correction was used in statistical analysis test. *P < 0.05, **P < 0.01, ***P < 0.005, and not significant by P > 0.05. Scale bar 10 μm

Transcriptomic response to peptide treatment in prostate cancer cells

To further uncover the molecular basis underpinning the effects of **RSM3** on cancer cell viability, we next performed bulk RNA-seq in PC3 cells treated with vehicle or 25 μM **RSM3** for 12 h (**Fig. 6a**). Interestingly, we identified only 89 differentially expressed genes (DEGs; |FC≥2| and FDR = 0.05) in the **RSM3** *vs.* control group comparison, indicating a highly specific transcriptomic response to m6A pathway disruption. At a less stringent threshold of FC≥1.5, 302 DEGs were detected, including 202 upregulated and 100 downregulated (**Fig. 6a**), which could be reasonably interpreted as a result of blocking m6A function in promoting mRNA decay [34]. GO analysis of these 302 DEGs by Metascape implied that the upregulated genes were enriched in pathways involved in programmed cell death, p53 tumor suppressor signaling, differentiation, and immunity (**Fig. 6b**), whereas down-regulated genes were mainly enriched in pathways involved in promoting cancer aggressiveness, stemness, and proliferation (**Fig. 6c**). These findings were generally consistent with our recent study that oncogenic function of the m6A pathway in prostate cancer was associated with features of tumor immune microenvironment (*e.g.* cytokine signaling)[35]. Gene set enrichment analysis (GSEA) further confirmed the GO results, showing that expression of apoptosis, inflammatory response, and p53 signaling signature genes was enriched in **RSM3**-treated cancer cells (**Fig. 6d**). In addition, the androgen receptor (AR) pathway was significantly enriched in AR^- PC3 cells after **RSM3** treatment (**Fig. 6e**), indicating that METTL3 inhibition by **RSM3** might be accompanied by restoration of aggressive AR^- cells to a more indolent AR^+ cell state. Real-time qPCR analysis was used to validate the results of RNA-seq analysis (**Fig. 6f**), which showed upregulation of NF-κB responsive genes related to inflammation and apoptosis and downregulation of genes related to cell cycle and proliferation. In particular, the expression of luminal differentiation genes (i.e., AR, PSA, NKX3.1, CK18) was increased while expression of stemness genes decreased, further supporting the molecular differentiation phenotype associated with **RSM3** treatment (**Fig. 6f**). To verify that the effects of **RSM3** treatment were due to inhibition of m6A signaling, we checked for overlap between DEGs detected by this RNA-seq analysis and either human m6A-targeted genes recorded in the M6A2Target database [36] (**Fig. 6g**) or METTL3-bound proteins (**Fig. 6h**) identified by RIP-seq in our parallel study (FYQ-paper). This analysis showed that DEGs detected in **RSM3**-treated PCa cells were indeed significantly enriched with genes subject to m6A modulation, thus illustrating the on-target effects of METTL3 inhibition by **RSM3**. Furthermore, we also noted that MAPK signal cascade genes were dramatically overrepresented among the upregulated GO terms in **RSM3**-treated cells (**Fig. 6b**), implying that **RSM3** may deactivate MAPK activity. Western blot analysis further showed lower phosphorylation levels of p42/44 in the **RSM3** group (**Fig. 6i**), indicating that **RSM3** treatment resulted in decreased activity of ERK/MAPK. Collectively, our data supported that METTL3 inhibition by **RSM3** could retard cancer cell growth and evoked apoptosis via inhibition of MAPK mitotic pathway, together with induction of differentiation, in an m6A-dependent manner.

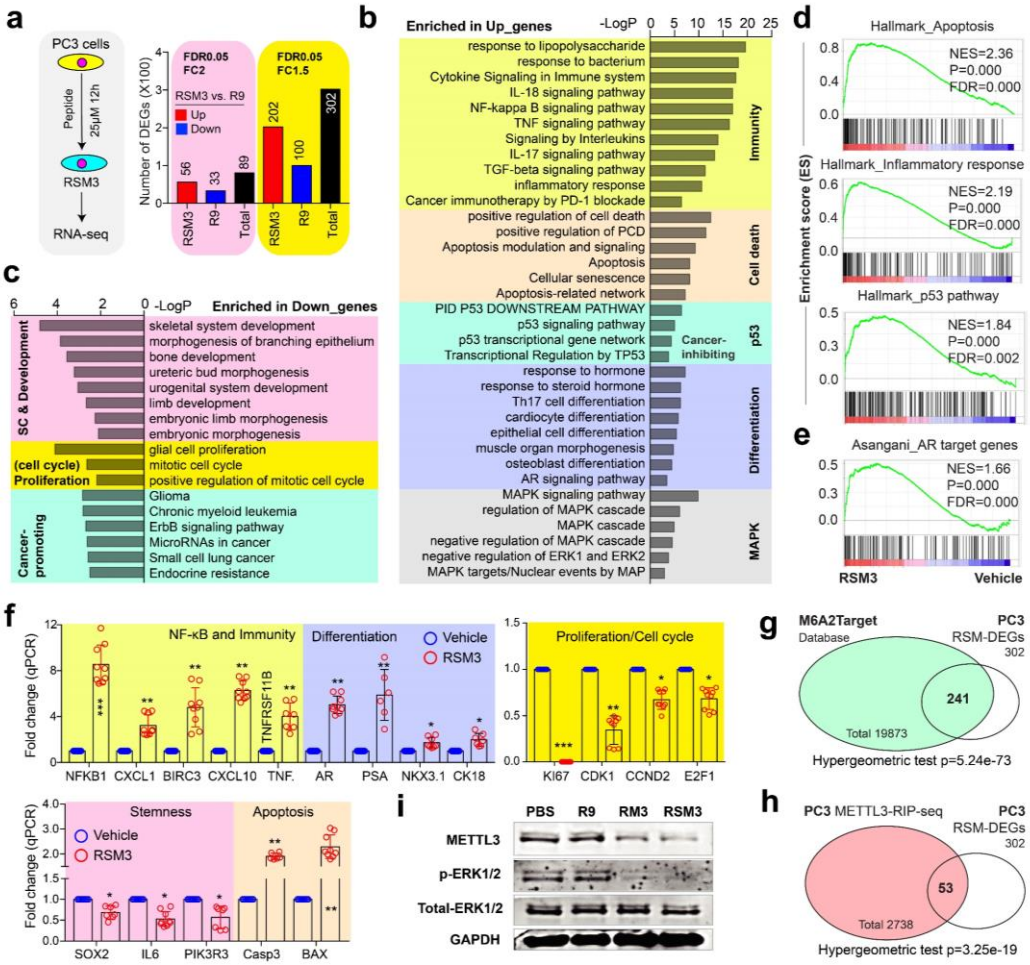

Figure 6. Molecular impact of METTL3-targeting peptide on cancer cell transcriptome. (a) Effect of **RSM3** on PCa transcriptome *in vitro*. Shown are schema of RNA-seq experiments (left) and total DEGs (right) identified by two different but stringent statistical thresholds. GO analysis of upregulated **(b)** and downregulated **(c)** DEGs in PC3 cells treated with or without **RSM3**. Terms with p-value <0.01, minimum count 3, and enrichment factor >1.5 (the ratio between observed count and the count expected by chance) were considered significant. The terms with similar descriptions and functions were grouped into different functional categories. **(d) and (e)** GSEA showing enrichment of the indicated gene signature in **RSM3**- *vs*. vehicle-treated PC3 cells. **(f)** qPCR analysis of indicated genes in PC3 cells treated with or without **RSM3**. Overlap between 302 DEGs and human m6A-targeted genes in M6A2Target database (**g**) and METTL3-bound genes identified in PC3 cells (**h**). Statistics was calculated by hypergeometric test. **(I)** Western blot analysis of p42/44 MAPK phosphorylation in PC3 cells treated with vehicle or peptide inhibitors at 25 μM for 12 h. For **f** mean and error (±s.d.) were obtained from at least three replicates. One-way analysis of variance (ANOVA) with Tukey's test correction was used in statistical analysis test. *P < 0.05, **P < 0.01, ***P < 0.005, and not significant by P > 0.05

RSM3 safety and anti-tumor efficacy in vivo

To assess safety, we examined its acute toxicity *in vivo* through a single intraperitoneal injection of **RSM3** (50 mg/kg) into C57/BL mice. After 24 h, routine blood analysis showed no significant differences in WBC, PLT, or RBC levels between mice injected with **RSM3**

and those injected with **RM3**, **R9**, or PBS. Although HGB levels were significantly lower in the **RSM3** group compared to the PBS control group, HGB values remained within acceptable limits (**Fig. 7a**). Histopathological examination of major organs, including the heart, liver, spleen, lung, and kidney, from mice treated with the peptide inhibitors, showed no significant abnormalities or lesions in any treatment groups (**Fig. S7**). These results strongly suggested that the peptide inhibitors conferred no obvious toxicity to mice.

We then evaluated the anti-cancer activity of **RSM3** in PC3 xenograft tumor model. Tumor-bearing mice were given a single peri-tumoral injection of 100 μL **RM3**, **RSM3** (20 mg/kg), or the R9 or PBS control components, every two days for two weeks. Measurements of tumor size and mouse body weight throughout the 2-week experimental period indicated that **RSM3** or **RM3** treatment resulted in significant suppression of tumor growth compared to the R9 or PBS control groups (**Fig. 7b)**. More specifically, tumor volumes were 2~3 fold smaller in the **RSM3** group compared to controls, with the stapled **RSM3** peptide exhibiting higher efficacy than the non-stapled **RM3** peptide, suggesting that increased stability through stapling could enhance the peptide inhibitory activity *in vivo*. Throughout the therapeutic course, the body weights were unaffected in all groups, and histopathological examination of organs (heart, liver, spleen, lung, kidney) found no significant abnormalities or lesions, indicating that none of the compounds had noticeable toxicity in the tumor-bearing mice (**Fig. S8**).

Immunohistochemical analysis of tumor samples showed that treatment with either **RM3** or **RSM3** resulted in a ~50% reduction in METTL3 expression and m^6A levels compared to the R9 and PBS groups. Additionally, caspase-3 expression increased by ~1.8-fold, while Ki67 decreased by ~65%, indicating that tumor growth was likely suppressed in the **RSM3** or **RM3** groups via induction of apoptosis and inhibition of proliferation (**Fig. 7c**). Furthermore, using the ASPC-1 cell line and ASPC-1 xenograft tumor model of pancreatic cancer to evaluate generalizability of peptide inhibitors, we found that **RSM3** also exhibited substantial anti-tumor activity towards ASPC-1 cells (**Fig. S9**, IC_{50} = 33.8 ± 7.0 μM) and ASPC-1 xenograft tumors (**Fig. S10)**, with significantly lower tumor volumes, and ~50% lighter tumor weights in the **RSM3**-treated group compared to the PBS- and R9-treated control groups. We speculated that these observations might be due to a common role of METTL3 in promoting pancreatic cancer development and metastases[37].

Based on our above findings, we next sought to compare the anti-tumor effects of **RSM3** with that of the previously reported small molecule inhibitor of METTL3, **STM2457** [19]. Both **STM2457** and **RSM3** exhibited potent toxicity towards PC3 and DU145 cells (**Fig S11**), and RSM3 displayed higher toxicity, with lower IC_{50} values, than the **STM2457** in PC3 (26.5 ± 1.2 *vs* 95.5 ± 3.6, **RSM3** *vs* **STM2457**) and DU145 (33.6 ± 1.5 *vs* 149.3 ± 10.1, **RSM3** *vs* **STM2457**) cells. Subsequent RNA blot assays revealed a significant reduction in m6A levels in PC3 cells treated with either **RSM3** or **STM2457**. Notably, **RSM3** exhibited a marginally superior m6A inhibition effect compared to **STM2457** (**Fig. S12**). To this end, **STM2457** or **RSM3** were administered to PC3 xenograft model mice at the same dosage (20 mg/kg), which demonstrated that both **STM2457** and **RSM3** could effectively suppress tumor growth in PCa tumors *in vivo* (**Fig. S13).** However, tumor mass was significantly lower in the **RSM3** group compared to **STM2457**-treated tumors (**Fig. S12c**), that is,

average tumor mass in the **RSM3** group was ~37% that in the PBS group, while average tumor mass in the **STM2457** group was 70% that of controls. These results demonstrated that peptide inhibitors of METTL3 can effectively suppress prostate and pancreatic tumor development *in vivo*. Moreover, these findings in xenograft tumor model supporting the potent disruption of METTL3 activity and stability by **RSM3** suggest that these peptide inhibitors function through a different and potentially more reliable pathway than small molecule METTL3 inhibitors.

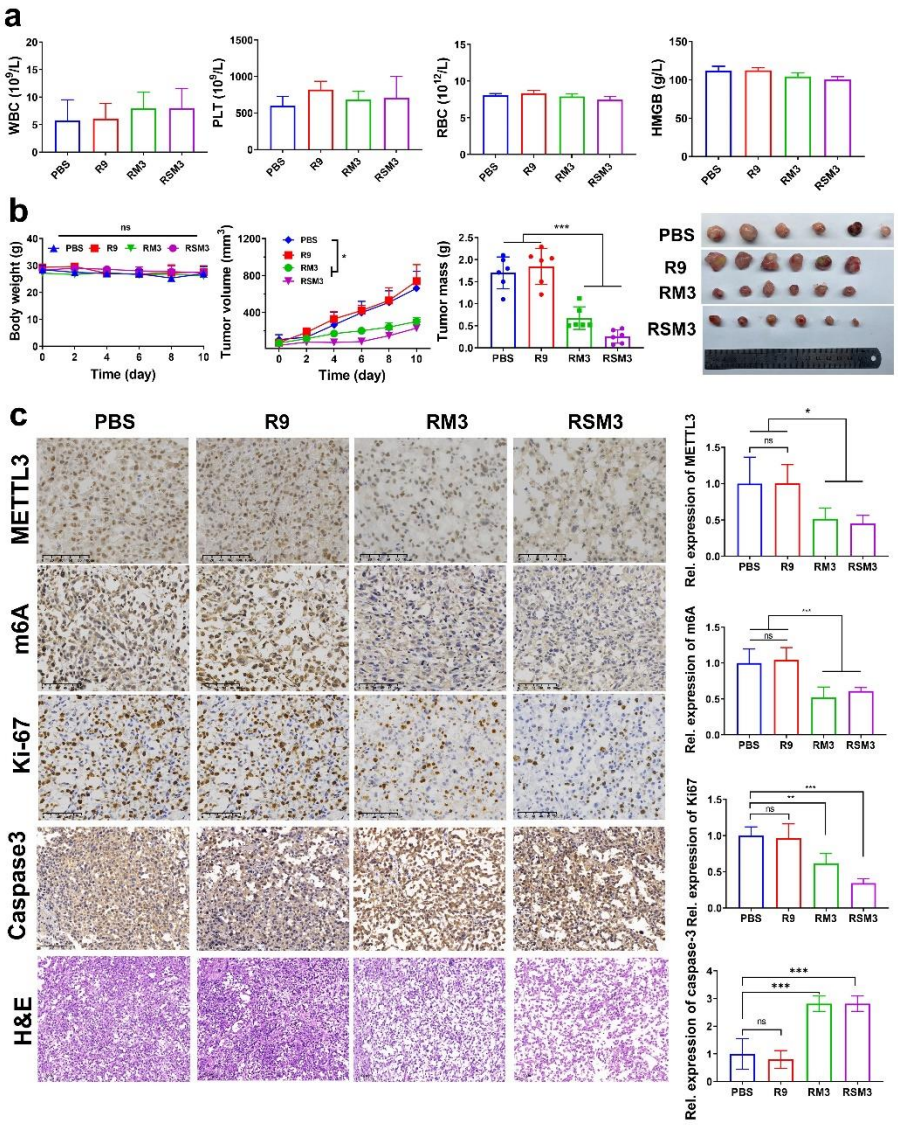

Figure 7. Toxicity and anti-tumor efficacy studies of peptide inhibitors. (a) Blood routine analysis (WBC, PLT, RBC, HMGB) of C57/BL mice after a single administration of 50 mg/kg **RSM3** to assess the toxicity of the peptide inhibitor. (b) The change in body weight and tumor index (including tumor volume and tumor mass) was recorded and analyzed during the therapeutic process to demonstrate the tumor-suppressive effects of the peptide inhibitor in the PC3 cells xenograft tumor model. (c) Immunohistochemistry (IHC) image and quantification of expression analysis of METTL3, Ki67, caspases-3 and m^6A in PC3 cells xenograft mice tumor tissue after peritumoral injecting with peptide inhibitor (20 mg/kg) for 10 days. For **a-c** mean and error (±s.d.) were obtained from at least three replicates. One-way analysis of variance (ANOVA) with Tukey's test correction was used in statistical analysis test. *$P < 0.05$, **$P < 0.01$,

***P < 0.005, and not significant by P > 0.05.

Conclusion

Our current study focused on the development of a bhp-linked stapled peptide inhibitor targeting the m6A methyltransferase, METTL3, in cancer cells. Comprehensive physicochemical and functional characterization in multiple cancer cell lines *in vitro* demonstrated that the **RSM3** stapled peptide displayed relatively high affinity towards the METTL3 binding site for complex formation with METTL14, reasonably high stability in denaturing conditions compared to other candidates, and significant cytotoxicity and anti-tumor activity *in vitro* and *in vivo*. Notably, **RSM3** binding with METTL3 not only disrupted its activity, but also activated its proteasomal degradation, resulting in substantially reduced mRNA m^6A global methylation levels, *in vitro* and *in vivo*. In treatments of two different prostate cancer cell lines, **RSM3** exhibited potent inhibition of cell proliferation and migration, supporting its potential as a therapeutic agent. Transcriptomic analysis indicated that **RSM3** could trigger inflammatory response pathways, activating p53 signaling, ultimately inducing cell cycle arrest and ultimately programmed cell death via apoptosis. We also validated that **RSM3** deactivates MAPK signaling. In PC3 Xenograft Model mice, treatment with **RSM3** twice a day of 20mg/kg could reduce METTL3 expression and promote apoptosis in the tumor microenvironment *in vivo*, thus providing compelling evidence if its efficacy. Furthermore, **RSM3** could provide significantly higher cytotoxicity and anti-tumor activity towards prostate cancer *in vivo* and *in vitro* compared to the small molecule METTL3 inhibitor, **STM2457**, potentially due to differences in the mechanism of action. The combined properties of high METTL3 inactivation and prolonged stability in the tumor cells collectively support the potential for broad application and generalizability of **RSM3** in treating a range of METTL3-dependent cancers [15]. In addition, the innovative design strategy for **RSM3** provides a theoretical framework for developing future research tools and targeted therapies, including other diseases linked to dysregulation of m6A methylation, with broader implications for targeting other complexes with oncogenic function in future therapeutic development.

Funding Sources

This work was supported by the National Natural Science Foundation of China (21975068 to J.S. and 81972418 to D.Z.), the National Youth Talent Support Program (202309460011), Natural Science Foundation of Hunan (2020RC3017 and 2022JJ10008 to J.S., 2021JJ10028 to D.Z.), Shenzhen Science and Technology Program (JCYJ20210324122403010 to J.S., JCYJ20220530160410024 to D.Z.).

Data Availability

The RNA-seq data have been deposited in GEO database under accession code GSE241315 and GSE240668.

Notes

J.S, D.Z, Y.F, M.W, and H.H are inventors on pending patent applications (No. 202211104956.7, and 202211105358.1), the authors declare no other competing financial

interest.

ACKNOWLEDGMENT

We would like to thank the Analytical Instrumentation Center of Hunan University for Assistance in Confocal Microscopy.

REFERENCES

1. Fu Y, Dominissini D, Rechavi G, He C. Gene expression regulation mediated through reversible m(6)A RNA methylation. *Nat Rev Genet* 2014, **15**(5)**:** 293-306.
2. Lee M, Kim B, Kim VN. Emerging roles of RNA modification: m(6)A and U-tail. *Cell* 2014, **158**(5)**:** 980-987.
3. Jiang X, Liu B, Nie Z, Duan L, Xiong Q, Jin Z*, et al.* The role of m6A modification in the biological functions and diseases. *Signal Transduct Target Ther* 2021, **6**(1)**:** 74.
4. Meyer KD, Jaffrey SR. Rethinking m(6)A Readers, Writers, and Erasers. *Annu Rev Cell Dev Biol* 2017, **33:** 319-342.
5. Liu J, Yue Y, Han D, Wang X, Fu Y, Zhang L*, et al.* A METTL3-METTL14 complex mediates mammalian nuclear RNA N6-adenosine methylation. *Nat Chem Biol* 2014, **10**(2)**:** 93-95.
6. Wang P, Doxtader KA, Nam Y. Structural Basis for Cooperative Function of Mettl3 and Mettl14 Methyltransferases. *Mol Cell* 2016, **63**(2)**:** 306-317.
7. Lin S, Choe J, Du P, Triboulet R, Gregory RI. The m(6)A Methyltransferase METTL3 Promotes Translation in Human Cancer Cells. *Mol Cell* 2016, **62**(3)**:** 335-345.
8. Lan Q, Liu PY, Haase J, Bell JL, Huttelmaier S, Liu T. The Critical Role of RNA m(6)A Methylation in Cancer. *Cancer Res* 2019, **79**(7)**:** 1285-1292.
9. Vu LP, Pickering BF, Cheng Y, Zaccara S, Nguyen D, Minuesa G*, et al.* The N(6)-methyladenosine (m(6)A)-forming enzyme METTL3 controls myeloid differentiation of normal hematopoietic and leukemia cells. *Nat Med* 2017, **23**(11)**:** 1369-1376.
10. Chen M, Wei L, Law CT, Tsang FH, Shen J, Cheng CL*, et al.* RNA N6-methyladenosine methyltransferase-like 3 promotes liver cancer progression through YTHDF2-dependent posttranscriptional silencing of SOCS2. *Hepatology* 2018, **67**(6)**:** 2254-2270.
11. Wang Q, Chen C, Ding Q, Zhao Y, Wang Z, Chen J*, et al.* METTL3-mediated m(6)A modification of HDGF mRNA promotes gastric cancer progression and has prognostic significance. *Gut* 2020, **69**(7)**:** 1193-1205.
12. Wang H, Deng Q, Lv Z, Ling Y, Hou X, Chen Z*, et al.* N6-methyladenosine induced miR-143-3p promotes the brain metastasis of lung cancer via regulation of VASH1. *Mol Cancer* 2019, **18**(1)**:** 181.
13. Li T, Hu PS, Zuo Z, Lin JF, Li X, Wu QN*, et al.* METTL3 facilitates tumor progression via an m(6)A-IGF2BP2-dependent mechanism in colorectal carcinoma. *Mol Cancer* 2019, **18**(1)**:** 112.
14. Li Y, Zhu S, Chen Y, Ma Q, Kan D, Yu W*, et al.* Post-transcriptional modification of m(6)A methylase METTL3 regulates ERK-induced androgen-deprived treatment resistance prostate cancer. *Cell Death Dis* 2023, **14**(4)**:** 289.
15. Zeng C, Huang W, Li Y, Weng H. Roles of METTL3 in cancer: mechanisms and therapeutic targeting. *J Hematol Oncol* 2020, **13**(1)**:** 117.

16. Xu P, Ge R. Roles and drug development of METTL3 (methyltransferase-like 3) in anti-tumor therapy. *Eur J Med Chem* 2022, **230:** 114118.
17. Fiorentino F, Menna M, Rotili D, Valente S, Mai A. METTL3 from Target Validation to the First Small-Molecule Inhibitors: A Medicinal Chemistry Journey. *J Med Chem* 2023, **66**(3)**:** 1654-1677.
18. Wang X, Feng J, Xue Y, Guan Z, Zhang D, Liu Z*, et al.* Structural basis of N(6)-adenosine methylation by the METTL3-METTL14 complex. *Nature* 2016, **534**(7608)**:** 575-578.
19. Yankova E, Blackaby W, Albertella M, Rak J, De Braekeleer E, Tsagkogeorga G*, et al.* Small-molecule inhibition of METTL3 as a strategy against myeloid leukaemia. *Nature* 2021, **593**(7860)**:** 597-601.
20. Selberg S, Blokhina D, Aatonen M, Koivisto P, Siltanen A, Mervaala E*, et al.* Discovery of Small Molecules that Activate RNA Methylation through Cooperative Binding to the METTL3-14-WTAP Complex Active Site. *Cell Rep* 2019, **26**(13)**:** 3762-3771 e3765.
21. Dolbois A, Bedi RK, Bochenkova E, Muller A, Moroz-Omori EV, Huang D*, et al.* 1,4,9-Triazaspiro[5.5]undecan-2-one Derivatives as Potent and Selective METTL3 Inhibitors. *J Med Chem* 2021, **64**(17)**:** 12738-12760.
22. Lee JH, Choi N, Kim S, Jin MS, Shen H, Kim YC. Eltrombopag as an Allosteric Inhibitor of the METTL3-14 Complex Affecting the m(6)A Methylation of RNA in Acute Myeloid Leukemia Cells. *Pharmaceuticals (Basel)* 2022, **15**(4).
23. Li H, Zhang Q, Feng Q, You Q, Guo X. The development of small molecules targeting methyltransferase-like 3. *Drug Discovery Today* 2023, **28**(4).
24. Pelay-Gimeno M, Glas A, Koch O, Grossmann TN. Structure-Based Design of Inhibitors of Protein-Protein Interactions: Mimicking Peptide Binding Epitopes. *Angewandte Chemie International Edition* 2015, **54**(31)**:** 8896-8927.
25. Edwards RJ, Moran N, Devocelle M, Kiernan A, Meade G, Signac W*, et al.* Bioinformatic discovery of novel bioactive peptides. *Nat Chem Biol* 2007, **3**(2)**:** 108-112.
26. Yu J-j, Zhou D-d, Yang X-x, Cui B, Tan F-w, Wang J*, et al.* TRIB3-EGFR interaction promotes lung cancer progression and defines a therapeutic target. *Nat Commun* 2020, **11**(1).
27. Lai Y, Fois G, Flores JR, Tuvim MJ, Zhou Q, Yang K*, et al.* Inhibition of calcium-triggered secretion by hydrocarbon-stapled peptides. *Nature* 2022, **603**(7903)**:** 949-956.
28. Muttenthaler M, King GF, Adams DJ, Alewood PF. Trends in peptide drug discovery. *Nat Rev Drug Discov* 2021, **20**(4)**:** 309-325.
29. Zhu C, Li T, Wang Z, Li Z, Wei J, Han H*, et al.* MC1R Peptide Agonist Self-Assembles into a Hydrogel That Promotes Skin Pigmentation for Treating Vitiligo. *ACS Nano* 2023, **17**(9)**:** 8723-8733.
30. Akishiba M, Takeuchi T, Kawaguchi Y, Sakamoto K, Yu H-H, Nakase I*, et al.* Cytosolic antibody delivery by lipid-sensitive endosomolytic peptide. *Nature Chemistry* 2017, **9**(8)**:** 751-761.
31. Dong H, Wang M, Fan S, Wu C, Zhang C, Wu X*, et al.* Redox‐Regulated Conformational Change of Disulfide‐Rich Assembling Peptides. *Angewandte Chemie International Edition* 2022, **61**(44).
32. Muppidi A, Doi K, Edwardraja S, Drake EJ, Gulick AM, Wang H-G*, et al.* Rational

Design of Proteolytically Stable, Cell-Permeable Peptide-Based Selective Mcl-1 Inhibitors. *Journal of the American Chemical Society* 2012, **134**(36)**:** 14734-14737.

33. Li YP, He XN, Lu X, Gong ZC, Li Q, Zhang L*, et al.* METTL3 acetylation impedes cancer metastasis via fine-tuning its nuclear and cytosolic functions. *Nat Commun* 2022, **13**(1)**:** 6350.

34. Lee Y, Choe J, Park OH, Kim YK. Molecular Mechanisms Driving mRNA Degradation by m(6)A Modification. *Trends Genet* 2020, **36**(3)**:** 177-188.

35. Zou C, He Q, Feng Y, Chen M, Zhang D. A m(6)Avalue predictive of prostate cancer stemness, tumor immune landscape and immunotherapy response. *NAR Cancer* 2022, **4**(1)**:** zcac010.

36. Deng S, Zhang H, Zhu K, Li X, Ye Y, Li R*, et al.* M6A2Target: a comprehensive database for targets of m6A writers, erasers and readers. *Brief Bioinform* 2021, **22**(3).

37. Lin C, Li T, Wang Y, Lai S, Huang Y, Guo Z*, et al.* METTL3 enhances pancreatic ductal adenocarcinoma progression and gemcitabine resistance through modifying DDX23 mRNA N6 adenosine methylation. *Cell Death & Disease* 2023, **14**(3).

Supporting Information

of

A Stapled Peptide Inhibitor of METTL3-METTL14 for Cancer Therapy

Zenghui Li[1,2,#], Yuqing Feng[1,3,#], Hong Han[1,2], Xingyue Jiang[1,2], Weiyu Chen[1,2], Xuezhen Ma[1], Yang Mei[1], Xuhui Yan[4], Ping Yin[4], Dan Yuan[1,2], Dingxiao Zhang[1, 3]*, Junfeng Shi[1,2,3,*]

[1] Hunan Provincial Key Laboratory of Animal Models and Molecular Medicine, State Key Laboratory of Chemo/Bio-Sensing and Chemometrics, School of Biomedical Sciences, Hunan University, Changsha, Hunan 410082, China

[2] Greater Bay Area Institute for Innovation, Hunan University, Guangzhou 511300, Guangdong Province, China

[3] Shenzhen Research Institute, Hunan University, Shenzhen 518000, Guangdong Province, China

[4] National Key Laboratory of Crop Genetic Improvement, Hubei Hongshan Laboratory, Huazhong Agricultural University, Wuhan, 430070, China.

Table of Contents

Materials and Experimental Methods

Figure S1. HPLC and mass spectra of peptides studied.

Figure S2. Synthetic routes of staple peptides.

Figure S3. The MTT assay determinate the cytotoxicity of peptide inhibitors towards multiple cancer cell lines.

Figure S4. Flow cytometry analysis investigating the effect of peptide inhibitors on the cell cycle.

Figure S5. WB analysis detecting the activation of caspase3 in PC3 after peptide inhibitors treatment.

Figure S6. CPP mixed with **SM3** for delivery peptide inhibitor into A549 cell.

Figure S7. H&E staining of organ sections from C57/BL mice.

Figure S8. H&E staining of organ sections from PC3-xenograft mice.

Figure S9. The MTT assay determinate the cytotoxicity of peptide inhibitors towards pancreatic cancer cell ASPC-1.

Figure S10. Peptide inhibitor suppresses tumor growth in pancreatic cancer cell ASPC-1 xenograft tumor model.

Figure S11. Cytotoxicity of **RSM3** compared to small molecular inhibitor **STM2457** in a prostate cancer model.

Figure S12. RNA blot assay showing the different impact of **RSM3** and **STM2457** on m6A methylation level in PC3 cells.

Figure S13. Therapeutic effect of **RSM3** compared to small molecular inhibitor **STM2457** in a prostate cancer model.

Supporting References

Materials and Experimental Methods

Materials

Rink Amide (AM) Resin, Fmoc-protected amino acids and O-Benzotriazole-N, N, N', N'-tetramethyl-uronium-hexaf (HBTU) were purchased from Hitch Biotech Shanghai Co., Ltd. Trifluoroacetic acid (TFA), acetonitrile, methanol, hexane, piperidine, and purified water were purchased from Yi nuo kai. All the solvents and reagents were used directly as received from commercial sources without further purification.

Peptide Synthesis

All peptides were synthesized by standard Fmoc solid-phase peptide synthesis on a CSBio 136S peptide synthesizer, with Rink Amide AM Resin and activation by HCTU. After the synthesis of the peptide chain, the resin should be washed successively with DMF, DCM, MEOH and n-hexane, Finally, the peptide chain without side chain protecting groups was cleaved from the resin with TFA/thioanisole/H_2O (95:2.5:2.5) for 3 h under nitrogen atmosphere. Crude peptide was obtained by concentrating the filtrate and precipitating it with cold ether. The crude product was purified by reversed phase high performance liquid chromatography (RP-HPLC) and lyophilized to obtain dry powder. All purified peptides were analyzed using analytical HPLC and MALDI-TOF MS.

Synthesis of SM3 and RSM3

Cross-linking reactions were performed by incubating M3 and RM3 peptides with 1.5 equivalents of P-bromo-methyl biphenyl (bhp) in a mixture of acetonitrile and 50 mM NH_4HCO_3 (1:1), pH 8.5, at a final peptide concentration of 1.0 mM. The reaction mixture was then incubated at room temperature for 2.0 h. The progress of the reaction was monitored using Analytical HPLC. Once the reaction was complete, the solvents were evaporated and any excess cross-linkers were removed by washing with diethyl ether. The cross-linked peptides were subsequently purified using preparative HPLC.

Circular Dichroism (CD)

CD spectra were obtained using a Jasco J-1500 spectrometer. Spectra were collected for

all peptides in a 1 mm quartz cell with wavelength and temperature dependence. Wavelength scans were taken at 1 nm step intervals with 3 s averaging time. Temperature-dependent wavelength scans were taken every 5 °C up to a maximum temperature of 70 °C with a 10 min equilibration time at each temperature. The 150 μM peptides were prepared in D.I. water and chilled on ice for at least 0.5 h. The mean residue ellipticity, [θ], was calculated using the following formula: $[\theta]=(\theta_{obs}/10lc)/r$, where θ_{obs} is the observed ellipticity in millidegrees, l is the length of the cell in centimeters, c is the concentration in molarity, and r is the number of residues.

Microscale Thermophoresis (MST) Assay

All measurements were conducted using the Monolith NT 115 instrument. Each measurement utilized a total volume of 10 μL loaded into standard capillaries. The ligand peptide was prepared by diluting it into a series of concentrations from a 5 mM stock solution. Prior to the measurements, the purified METTL3-METTL14 protein was diluted in assay buffer and labeled using the MO RED-NHS Protein Labeling Kit. After a 5-minute incubation period, the peptide inhibitors were added to achieve final concentrations of 50 nM for METTL3-METTL14 and a range of concentrations for the peptide inhibitor stock (ranging from 250 μM to 1.95 μM). Following an additional 10-minute incubation, the measurements were immediately taken using the same settings as previously described. The resulting data were processed using the MO Affinity Analysis software v2.3.

Serum Stability and Hemolysis Studies

Stability

Peptide were dissolved in 1:3 serum: buffer (20 mM Tris-HCl, 100 mM NaCl, pH 7.4) to a final concentration of 200 μM. Samples were then incubated at 37 °C in an incubator. At 0, 0.5, 1, 2, 4 or 8 h of incubation a 100 μL aliquot was removed and diluted with an equal volume of 15 wt% TCA in water, and the sample was kept on ice for 15 min. Samples were then centrifuged at 13,000 rpm for 10 min, and supernatant collected and subjected to analytical MS.

Hemolysis

Hemolysis investigations were conducted by procuring freshly drawn blood from healthy human volunteers into heparinized tubes, followed by subjecting it to centrifugation at a speed of 3,000 rpm for a duration of 10 minutes at a temperature of 4 °C. Red blood cells (RBCs) were subjected to three washes with a hemolysis buffer composed of 10mM Tris, 150 mM NaCl, pH 7.4. Subsequently, a solution of RBCs in the hemolysis buffer, with a concentration of 0.25% v/v, was meticulously prepared. In a 96-well plate, a volume of 75 μL of the RBC solution was admixed with an equivalent amount of a 2x peptide solution, previously dissolved in the hemolysis buffer, to initiate the assay. Negative and positive controls were established using a blank and a buffer containing 1% Triton-X100, respectively. The samples were subjected to incubation for a duration of 24 h, accompanied by gentle agitation. Subsequently, the plates were centrifuged at 4,000 rpm for 10 minutes at a temperature of 4 °C to precipitate intact RBCs. Following this, a volume of 100 μL of the supernatant from each well was extracted and transferred to an empty 96-well plate. The absorbance was then measured at a wavelength of 415 nm utilizing a microplate reader.

Cell Viability Assay

DU145 and PC3 cells were seeded in 96 plates at a density of 8000/well and continued to culture overnight at a 37°C, 5% CO2 incubator. Peptide stock solution was prepared in water and a series of concentrations of peptide work solution. Cells were incubated with peptide work solution for 24 h. Then the 100 μL 10 %v/v CCK8 solution was added to the plate well for 1 hour. After incubation, the plates were subjected to the UV plate reader to record 450 nm data. The absorbance of the negative controls was subtracted from each sample as a blank, and the percent viability was calculated as follows: (Absorbance peptide-treated cells / Absorbance untreated cells) ×100. GraphPad Prism 7.0 software was used to fit cytotoxicity curves and calculated IC_{50} values with a non-linear regression model.

Laser Scanning Confocal Microscope

Peptide uptake

Cells were seeded on 35 mm confocal dishes at a density of 8000/well and continued to culture for 24 h in a 37 °C incubator with 5% CO2. Then, the cells were washed twice with PBS buffer and incubated with 1mL peptide Prepared-work solution (30 μM) at 37 °C with 5 % CO2 for desired time. The incubated solution of cells was removed, and the following was washed twice. Then the cells were stained with 2 μg/mL Hoechst 33342 for 15 min, cell imaging was performed on an Olympus FV1200 microscopy with 60X oil objective, and the cells were maintained in a cell living imaging buffer during confocal imaging.

EdU Staining

The cells were cultured in 12-well plates at an appropriate density. Subsequently, the cells were treated with the 15 μM peptide inhibitor for the specified duration. To label proliferating cells, a 2 X EdU working solution (20 μM) pre-warmed to 37 °C was added to each well, resulting in a final concentration of 1 X EdU in the plate. The cells were then incubated for 2 h. After the EdU labeling period, the culture medium was removed, and 1 mL of fixative solution (PFA) was added to each well. The cells were fixed for 15 minutes at room temperature. The fixative solution was then removed, and the cells were washed three times. Finally, 0.5 mL of Click reaction solution was added to each well, and the plate was gently shaken to ensure even coverage of the sample. The images of the EdU staining were captured using the EVOSTM M5000 imaging system.

Tunel Staining

The cells were cultured in 12-well plates at an appropriate density. Following the treatment with the 15 μM peptide inhibitor for the designated time period, the cells were fixed using PFA and subjected to Tunel staining for 60 minutes at 37 ℃. DAPI staining was used to visualize the cell nuclei. The fluorescence microscope was utilized to count the number of Tunel-positive cells. The ratio of Tunel-positive cells to the total cell count was calculated to evaluate the level of cell apoptosis.

Cell Scratch Assay

The cells were seeded in a 12-well plate and cultured for a duration of 24 h, facilitating their

growth until reaching complete confluence. Then the scratch of cells was made across the cell monolayer using a sterile pipette tip. The detached cells were removed by washing with an FBS-free medium, and a fresh medium containing the desired treatment (peptide inhibitor or control molecule) was added. The cells were then incubated under appropriate conditions for 12 h, and finally images of the scratched area were captured using a microscope. The migration of cells into the scratched area was assessed by measuring the width of the different groups. The extent of cell migration was quantified using **ImageJ** software.

Western blotting (WB)

Cells were seeded into a 6-well plate at a density of $1x10^5$ cells per well and cultured for 24 h. Following treatment with the 15 μM peptide or inhibitor for the appropriate duration, the treated cells were lysed using 1x passive buffer supplemented with protease inhibitors such as PMSF and a phosphatase cocktail. The concentration of total protein in the lysates was determined using Quick Start Bradford 1x Dye Reagent, and the protein concentration was calculated accordingly. Subsequently, the protein samples were denatured by heating them at 95-100°C for 5 minutes and subjected to the Western blotting assay.

Peptide safety and Therapeutic Effect Study in Xenograft Models

All animal research conducted in this study was approved by the Ethics Committee for Animal Experiments at HNU University (Approval No. HNU-IACUC-2021-102).

Safety study

Six-week-old male C57/BL mice were procured from GemPharmatech LLC. (JiangSu). Following one week of acclimatization, the mice received a single injection of 50 mg/kg of the peptide. After 24 h, the mice were euthanized for the collection of organs and blood samples for subsequent analysis. The gathered data were further examined to assess the peptide safety.

Therapeutic Effect

Six-week-old male BALB/c nude mice were were purchased from GemPharmatech LLC. (JiangSu) for the study. PC3 cells were subcutaneously injected into the back of the mice at a density of $1x10^6$ cells in 50 μL PBS. Once the tumor volume reached approximately

100 mm^3, the mice were randomly divided into four groups and administered the drug once every two days at dosage of 20 mg/kg. The weight of the mice and the tumor volume were recorded every two days throughout the experiment. At the end of the study, the mice were euthanized, and tumor mass was measured. Organs and tumor tissue samples were collected for further analysis, including H&E staining and immunohistochemical analysis.

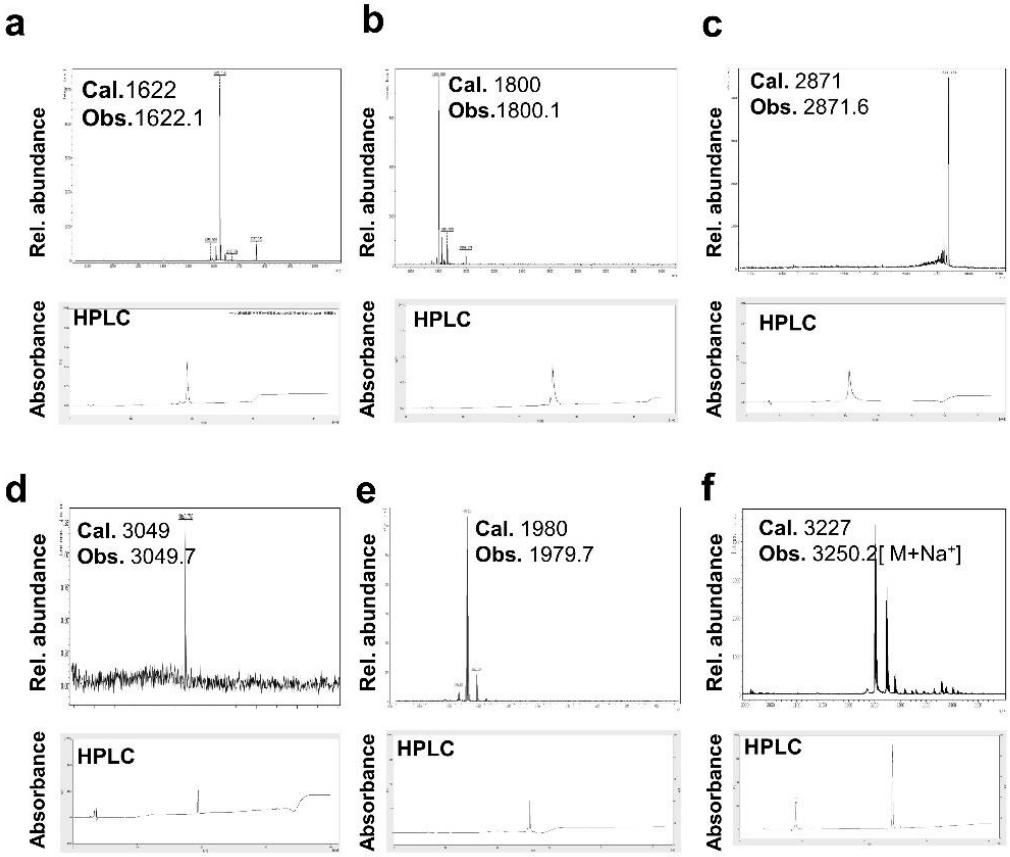

Figure S1. Analytic HPLC and mass spectra of all peptides studied. (a) **M3**, (b) **SM3**, (c) **RM3**, (d) **RSM3**, (e) **M3-FITC** and (f) **RM3-FITC** respective shown in this figure.

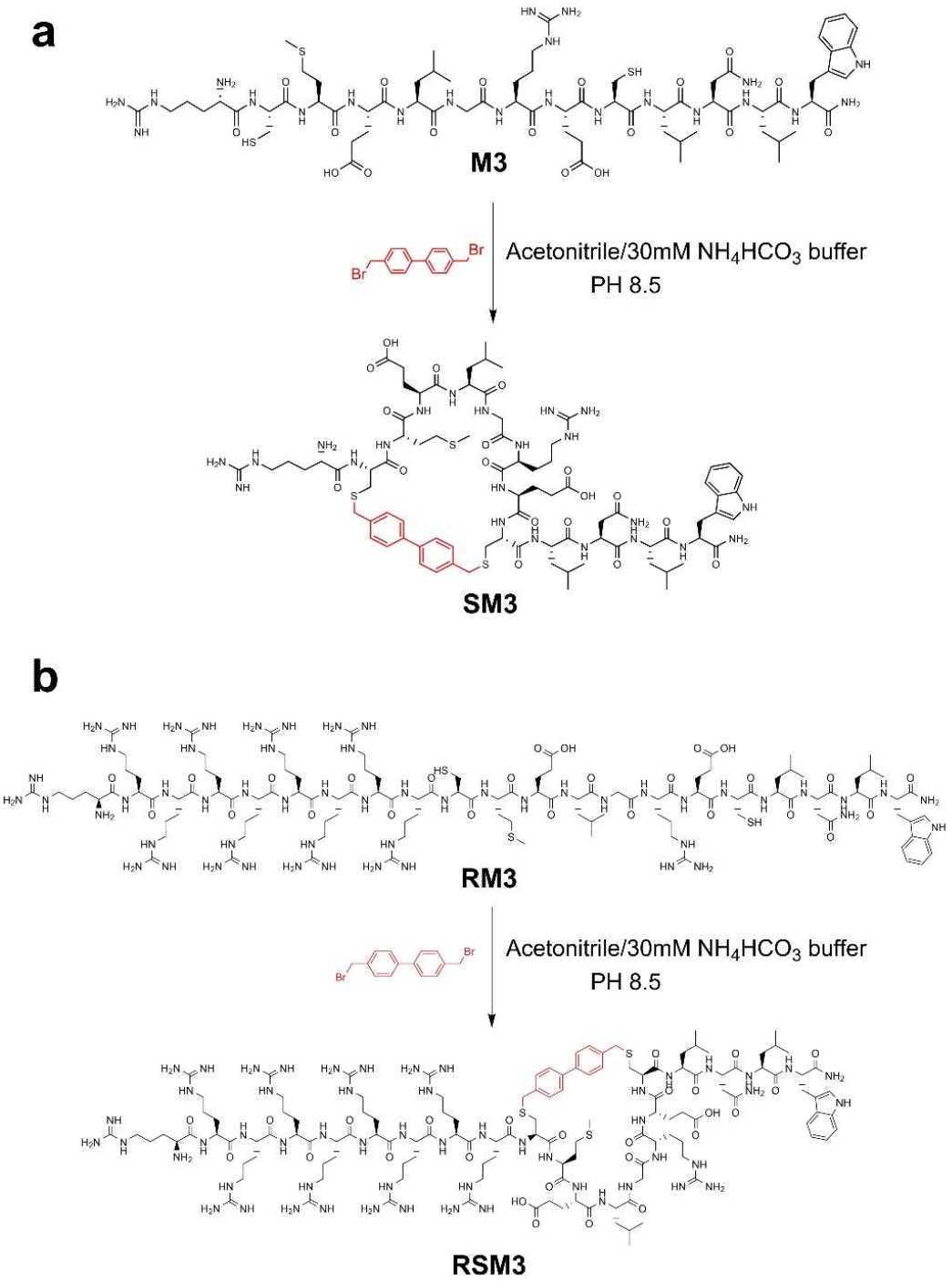

Figure S2. Synthetic routes of staple peptide **SM3** (A) and **RSM3** (B).

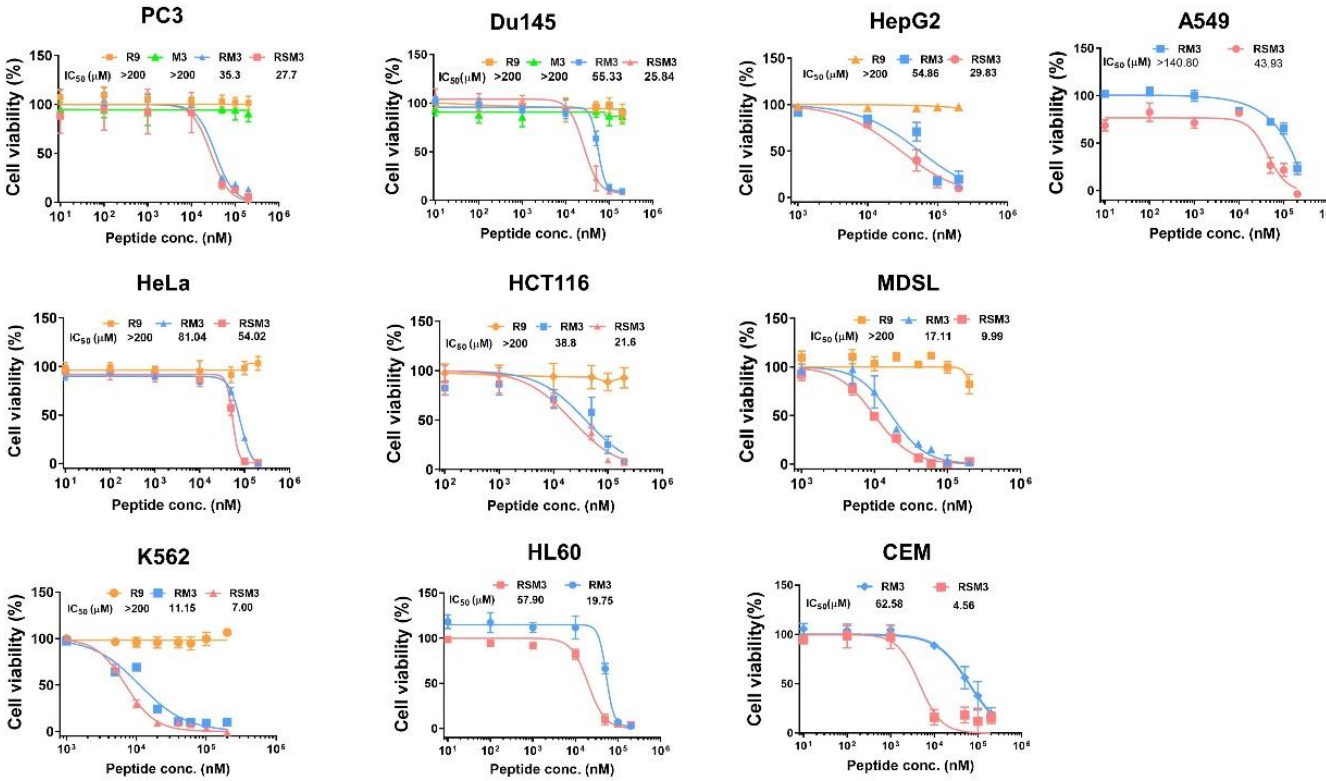

Figure S3. The MTT assay determinate the cytotoxicity of peptide inhibitors towards multiple cancer cell lines.

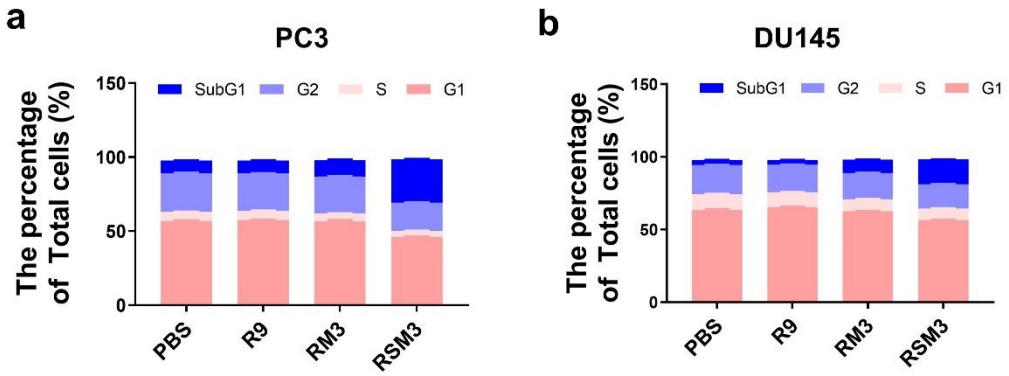

Figure S4. Flow cytometry analysis investigating the effect of **RSM3** (15 μM) on the cell cycle of (a) PC3 and (b) DU145 cells over 12 h.

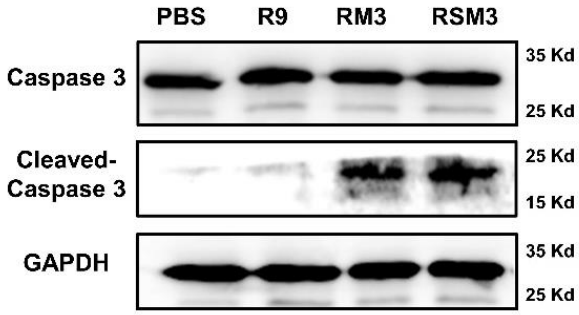

Figure S5. Western Blotting analysis of the activation of capase3 in PC3 cells after 15 μM peptide inhibitor treatment for 12 h.

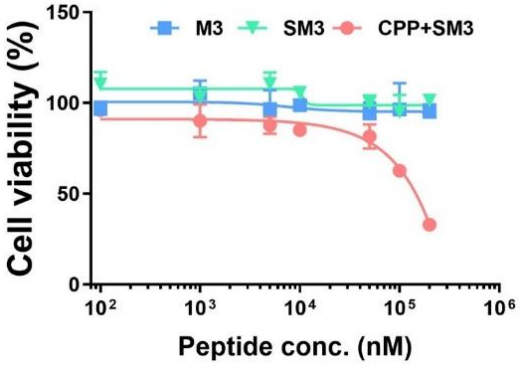

Figure S6. CPP mixed with **SM3** for delivery inhibitor into A549 cell.

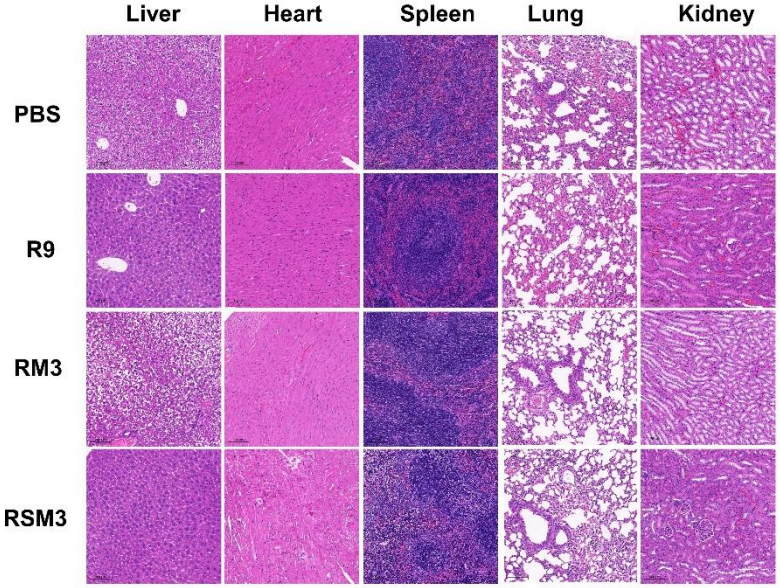

Figure S7. H&E staining of organ sections, including liver, heart, spleen, lung, and kidney, obtained from C57/BL mice after 50 mg/kg peptide treatment for 24 h, scale bar 100 μm.

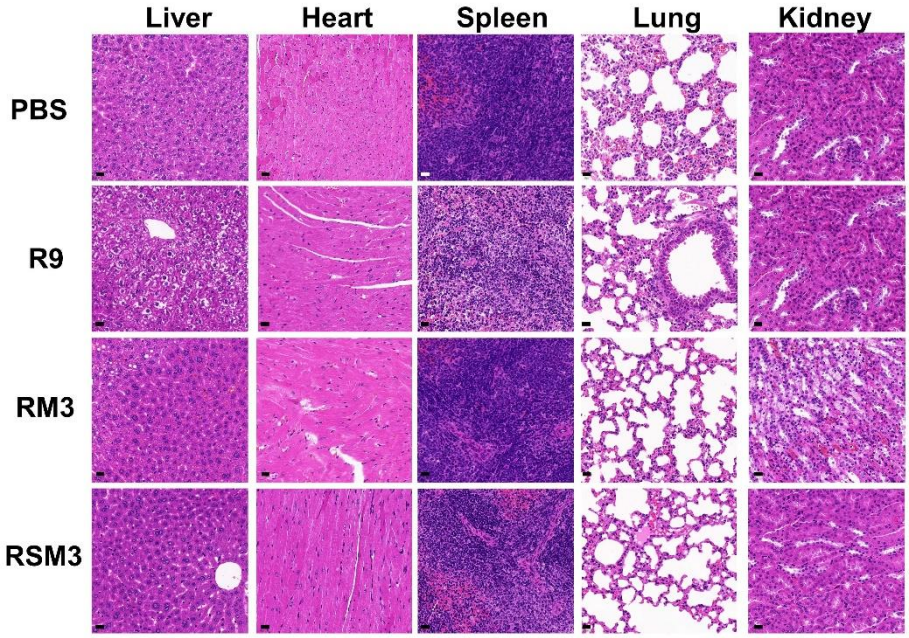

Figure S8. H&E staining of organ sections, including liver, heart, spleen, lung, and kidney, obtained from mice with PC3 cell xenograft tumors after 20 mg/kg peptide treatment for 10 days, scale bar 100 μm.

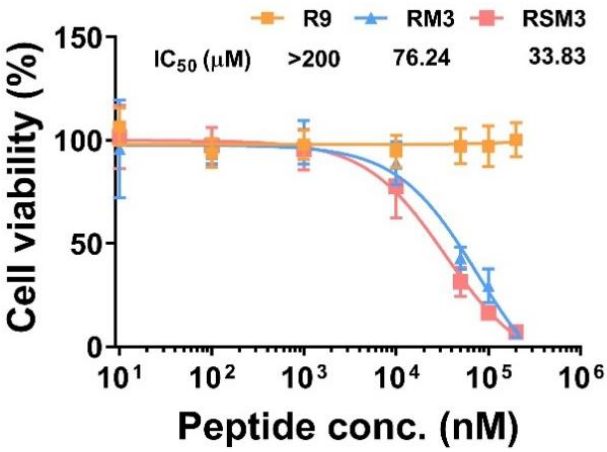

Figure S9. The MTT assay determinate the cytotoxicity of peptide inhibitors towards pancreatic cancer cell ASPC-1.

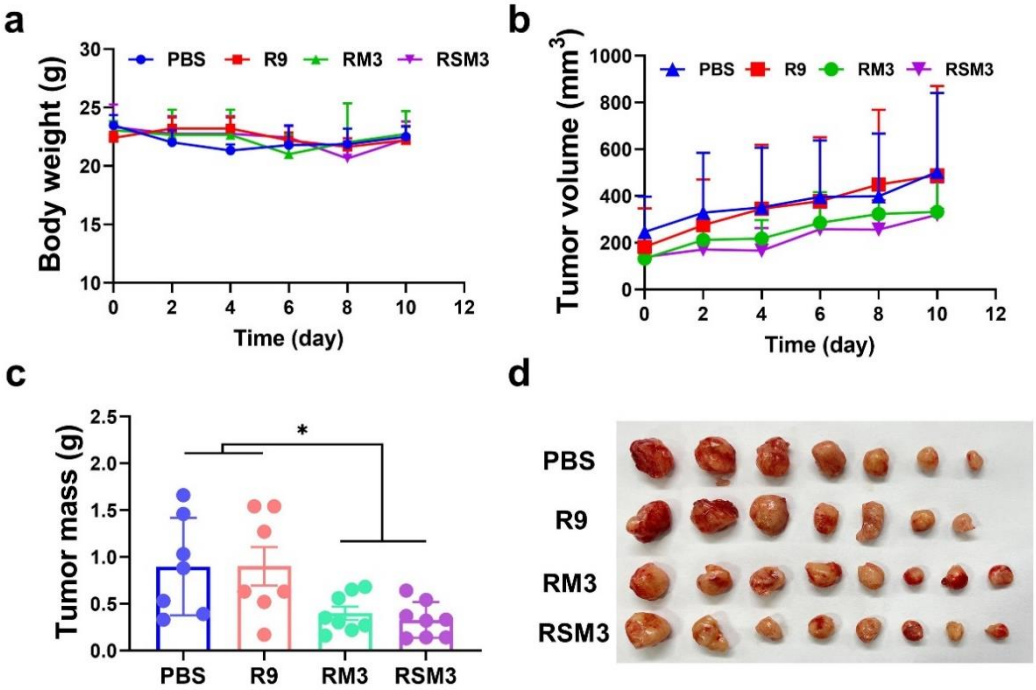

Figure S10. Peptide inhibitors suppress tumor growth in pancreatic cancer cell ASPC-1 xenograft tumor model. (a) Body weight of mice remained unchanged after treatment with peptides. (b) The tumor volume showed a reduction after different treatments. (c) Tumor mass after 10 days of treatment exhibited a notable decrease in **RM3** and **RSM3** group. (d) Images of sectioned tumors after 10 days of treatment displayed reduced tumor size in **RM3** and **RSM3** group. All peptides were administered at a dosage of 20 mg/kg in this assay. For **a-c** mean and error (±s.d.) were obtained from at least three replicates. One-way analysis of variance (ANOVA) with Tukey's test correction was used in statistical analysis test. *$P < 0.05$, **$P < 0.01$, ***$P < 0.005$, and not significant by $P > 0.05$.

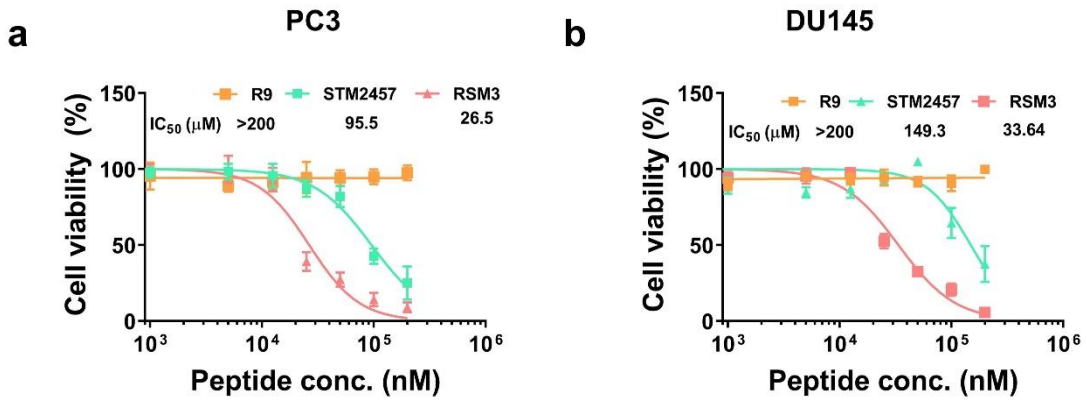

Figure S11. Cytotoxicity of **RSM3** compared to small molecular inhibitor **STM2457** in prostate cancer cell lines (A) PC3 and (B) DU145.

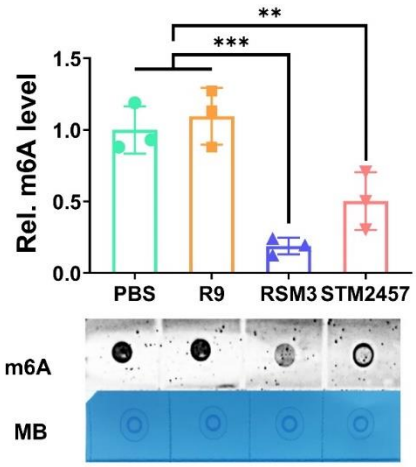

Figure S12. RNA blot assay(blow) and quantification (top) showing the different effects of **RSM3** and **STM2457** on m6A methylation level in PC3 cells. For mean and error (±s.d.) were obtained from three replicates. One-way analysis of variance (ANOVA) with Tukey's test correction was used in statistical analysis test. *P < 0.05, **P < 0.01, ***P < 0.005, and not significant by P > 0.05.

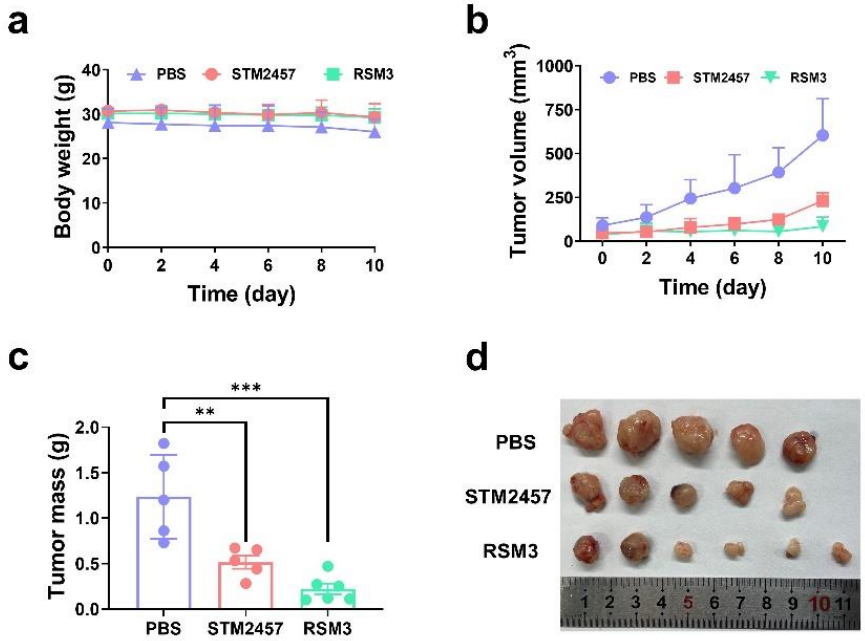

Figure S13. Therapeutic effect of **RSM3** compared to small molecular inhibitor **STM2457** in a prostate cancer model. (a) The Body weight of mice remained unchanged after treatment with both **STM2457** and **RSM3**. (b) The tumor volume showed a significant reduction after treatment with both inhibitors. (c) Tumor mass after 10 days of treatment exhibited a notable decrease in both **STM2457** and **RSM3** group. (d) Images of sectioned tumors after 10 days of treatment revealed reduced tumor size in **STM2457** and **RSM3** group. All molecules were administered at a dosage of 20 mg/kg in this assay. For **a-c** mean and error (±s.d.) were obtained from at least three replicates. One-way analysis of variance (ANOVA) with Tukey's test correction was used in statistical analysis test. *$P < 0.05$, **$P < 0.01$, ***$P < 0.005$, and not significant by $P > 0.05$.